Biophysical Journal
Article

Biophysical Society

Graphene Symmetry Amplified by Designed Peptide Self-Assembly

Gina-Mirela Mustata,[1] Yong Ho Kim,[2,3,*] Jian Zhang,[4] William F. DeGrado,[5] Gevorg Grigoryan,[4,6,*] and Meni Wanunu[1,*]

[1]Department of Physics, Northeastern University, Boston, Massachusetts; [2]SKKU Advanced Institute of Nanotechnology and Department of Chemistry, Sungkyunkwan University, Seoul, Korea; [3]Center for Neuroscience Imaging Research, Institute for Basic Science(IBS), Suwon, Korea; [4]Department of Computer Science, Dartmouth College, Hanover, New Hampshire; [5]Department of Pharmaceutical Chemistry, University of California San Francisco, San Francisco; and [6]Department of Biological Sciences, Dartmouth College, Hanover, New Hampshire

ABSTRACT We present a strategy for designed self-assembly of peptides into two-dimensional monolayer crystals on the surface of graphene and graphite. As predicted by computation, designed peptides assemble on the surface of graphene to form very long, parallel, in-register β-sheets, which we call β-tapes. Peptides extend perpendicularly to the long axis of each β-tape, defining its width, with hydrogen bonds running along the axis. Tapes align on the surface to create highly regular microdomains containing 4-nm pitch striations. Moreover, in agreement with calculations, the atomic structure of the underlying graphene dictates the arrangement of the β-tapes, as they orient along one of six directions defined by graphene's sixfold symmetry. A cationic-assembled peptide surface is shown here to strongly adhere to DNA, preferentially orienting the double helix along β-tape axes. This orientational preference is well anticipated from calculations, given the underlying peptide layer structure. These studies illustrate how designed peptides can amplify the Ångstrom-level atomic symmetry of a surface onto the micrometer scale, further imparting long-range directional order onto the next level of assembly. The remarkably stable nature of these assemblies under various environmental conditions suggests applications in enzymelike catalysis, biological interfaces for cellular recognition, and two-dimensional platforms for studying DNA-peptide interactions.

INTRODUCTION

In recent years, graphene and other two-dimensional (2D) crystals have emerged as a class of promising next-generation materials. Due to their size, strength, flexibility, and unique electronic properties, 2D materials are also intriguing as biological mimics, sensors, and building blocks for various applications in nanotechnology. However, because biological materials at all scales possess molecular diversity, specificity, and chirality, rational design of interfaces between 2D materials and the biological world requires tools that achieve precise interfacial molecular structure. Various strategies have already been used to generate functional graphene interfaces, ranging from covalent defect functionalization to molecular/biomolecular physisorption. In particular, considerable work has been performed toward characterizing peptides binding to graphitic surfaces (1–8). Peptide-based modifiers of nanomaterials are attractive because of the molecular diversity and chiral specificity they can enable (9). Previous approaches to graphene surface modification with peptides have relied on selection methods, such as phage display, to find sequences that effectively bind to graphene (10,11). In this work, we combine computational design and experiments to engineer and study peptide self-assembly on graphite and graphene. The crystalline, semihydrophobic graphene interface is utilized as a scaffold for self-assembled, atomically periodic monolayers of short polypeptides. Although we demonstrate the method using β-stranded peptides on graphene, it should be generally applicable to a variety of different conformations and surfaces. Experiments with these peptides reveal intriguing properties: the assemblies amplify the symmetry of underlying graphene by organizing along one of six directions dictated by graphene's sixfold symmetry; the 2D crystals are stable under a wide range of temperatures and pH/salt/urea concentrations; large domain sizes can be grown ($\sim 10^5$–10^6 molecules/domain); the assemblies shrink upon dehydration of the surface, fully recover their ordered structure upon rehydration, and are remarkably stable to proteinase K digestion; organization is sequence-dependent, although aromatic side chains are not required for assembly; and, finally, DNA assembly on cationic-peptide domains results

Submitted February 17, 2016, and accepted for publication April 8, 2016.

*Correspondence: yhkim94@skku.edu or gevorg.grigoryan@dartmouth.edu or wanunu@neu.edu

Editor: Wilma Olson.

http://dx.doi.org/10.1016/j.bpj.2016.04.037

in preferential DNA alignment with the domain structure. We first present our computational design approach, followed by our experimental findings of 2D self-organization on graphene and graphitic surfaces.

MATERIALS AND METHODS

Experiments

All peptides were purchased from Genscript (http://www.genscript.com/) at >98% purity (HPLC purified), and all buffers were prepared in ultrapure deionized water (Millipore, Billerica, MA). For pH study, a tricomponent buffer composed of citrate, HEPES, and CHES was used (broad-range buffer CHC; Molecular Dimensions, Altamonte Springs, FL). Highly oriented pyrolytic graphite (HOPG) slabs for imaging on graphite were purchased from SPI Supplies (Structure Probe, West Chester, PA). Atomic force microscopy (AFM) imaging was performed with a FastScan AFM instrument (Bruker Instruments, Billerica, MA) using soft triangular-shaped silicon nitride cantilevers (FastScan C, Bruker Instruments) characterized by a nominal spring constant of $k \sim 0.8$ N/m and a nominal resonant frequency of 300 kHz. Imaging was performed using the FastScan device's ScanAsyst Mode at speeds of ~4 lines/s for optimal topographic quality. For AFM imaging under fluid, we used a home-made perfusion cell that allowed the fluid medium to be refreshed.

Assembly modeling

The assembly optimization framework was implemented using the Molecular Software Library (12) in conjunction with the EEF1.1 implicit-solvent force field (13,14). In stage-one calculations, graphene-bound poses were explored by sampling backbone φ- and ψ-angles, side-chain χ-angles, elevation, and orientation relative to graphene. The latter was defined with two angles (i.e., rotation of the peptide around its own axis and the angle between this axis and graphene's surface) and elevation over graphene (optimized from the range 0–10 Å). Graphene-bound peptide poses from stage one, in the order of ascending energy, were considered in stage-two calculations, where P1 and P2 lattice parameters were searched through discrete optimization (Fig. 1; Supporting Materials and Methods in the Supporting Material). The best-found lattice parameters were used as input into a continuous minimization procedure via the Simplex algorithm of Nelder and Mead to minimize the total energy of a 5×5 peptide assembly fragment. The optimal assembly geometry resultant from this minimization was taken as the final best assembly geometry for the input graphene-bound pose.

Implicit-solvent molecular dynamics (MD) simulations were run using CHARMM 38b2 (15), at 298.15 K, with the EEF1.1 force field. Graphene atoms were fixed for the sake of efficiency. VALOCIDY calculations were performed as described earlier (16). Integration was carried out in the bond-angle-torsion coordinate system associated with the simulated peptide. Initial configurations for side-on and end-on peptide poses were taken from the modeling procedure above as the optimal single-peptide bound

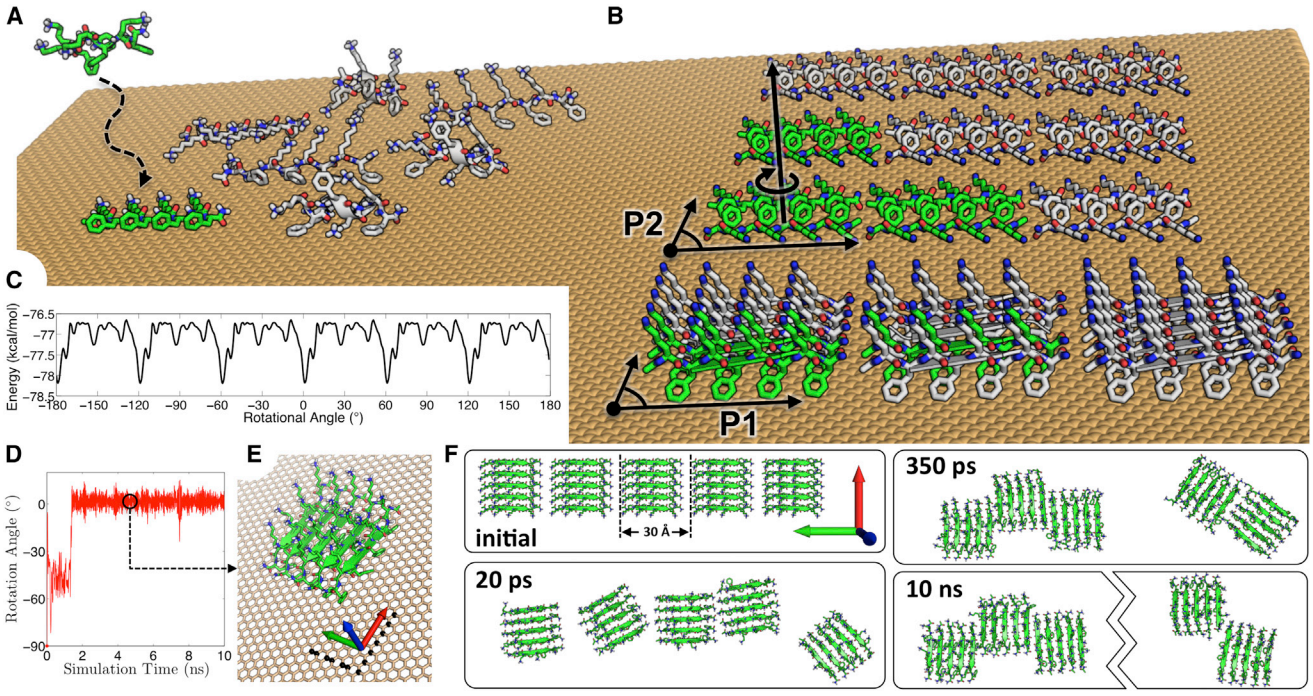

FIGURE 1 Assembly modeling procedure and results. (*A*) The first stage sampled peptide-graphene poses to simulate the process of a single peptide attaching to graphene (*green*) and exploring bound conformations (*gray*). (*B*) Approximately 8×10^5 lowest-energy poses found were passed onto the second stage, where 2D assembly parameters were optimized for space groups P1 and P2 (four parameters for P1 and six for P2, in addition to side-chain configurations; see Materials and Methods). Lowest-energy assembled states for these two space groups are shown on the bottom and top, respectively (a unit cell and two images are shown in *green*, with other images in *gray*), with the P1 assembly showing a substantially lower energy. This assembly preferentially aligns along specific axes on the graphene lattice, as evidenced by (*C*) the periodic potential energy landscape found in both ground-state modeling and (*D–F*) MD simulations of assembly fragments. Rotation angle was defined between the direction of β-strands and the laboratory *X* axis (*red* in *E*), with the laboratory *Y* axis (*green* in *E*) used to define the sign; some graphene atoms along both *X* and *Y* axes are shown as black spheres in (*E*). As evident from the MD-derived angular trajectory in (*D*), a five-strand assembly domain quickly settles on the optimal alignment expected from ground-state modeling (a representative snapshot shown in *E*), even though it is initially placed orthogonally to this orientation. (*F*) MD simulation of a larger assembly fragment placed on graphene orthogonally to the preferred orientation (graphene is hidden for clarity, but lattice direction is indicated by the axes in the first panel as in *E*; panels illustrate the initial conformation and MD snapshots from 20 ps, 350 ps, and 10 ns). Domains rapidly reorient along the optimal axis, while different interdomain lateral dockings are sampled. To see this figure in color, go online.

conformation and the conformation in the optimal assembly, respectively. Thermodynamic states were defined around these two poses as ensembles of conformations with φ/ψ backbone angles within 30° of their starting values and distances between peptide Cα atoms and the graphene plane within 2 Å of their starting values. During MD, these states were sampled by restraining dihedral angles and Cα-to-graphene distances with flat-bottom potentials using the MMFP module in CHARMM (15). The free energy of each state was computed by averaging estimates from 100 independent simulations with 1 ns of sampling time after 100 ps of equilibration. The side-on state was found to be preferred by 15.4 kcal/mol, while the standard deviations of the 100 estimates were 1.6 kcal/mol and 1.7 kcal/mol for the side-on and end-on poses, respectively, demonstrating good convergence.

Explicit-solvent simulations were performed in NAMD (17) in the NTP ensemble at 298.15 K and 1 atm, using CHARMM parameter set 22. A 60 × 50 Å section of graphene was fixed in the *X*,*Y* laboratory frame, centered at the origin, and modeled using the aromatic atom type CA with no partial charge. To remove bias toward a specific binding pose, the peptide was initially placed pointing along the laboratory *Z* axis in a fully extended conformation, with the peptide center of mass elevated by ~20 Å over graphene (the closest terminal atom of the peptide was within ~10 Å of graphene). The system was solvated with a box of TIP3 water, using 6 Å padding in all directions (a total of 6208 water molecules were included). To enrich sampling for graphene-bound conformations and to prevent edge effects, the center of mass of peptide Cα atoms was restrained to be within 15 Å of graphene along the *Z* axis and 3 Å from the origin within the *X*,*Y* plane. These restraints were encoded via the collective variable module in NAMD as half-harmonic potentials. Ten independent 10-ns MD simulations were run, with Fig. S3 summarizing the final state of each.

Modeling of DNA orientational preferences

All calculations were performed in CHARMM 38b2 (15), at 300 K, using the generalized-Born with a simple-switching-model method, previously shown to reproduce molecular electrostatics in close agreement with Poisson-Boltzmann theory (18). Model parameters were: half-smoothing length of 0.3 Å, nonpolar surface tension coefficients of 0.03 kcal·mol^{-1}·Å^{-2}, grid spacing of 1.5 Å, and 50 mM salt concentration (with remaining parameters kept at their default values). Long-range interactions were cut off at 9.5 Å, with the switching function starting at 8.5 Å. Both DNA and the peptide layer (either the ground-state structure or the perturbed assembly, as described in the main text) were treated as rigid bodies, and all six degrees of freedom of DNA with respect to the assembly were sampled. As DNA-peptide attraction was quite strong, multicanonical Monte Carlo simulation was used to assure thorough sampling of orientations (see Supporting Materials and Methods for implementation details). Data were collected from 100 independent trajectories, started with random placements of DNA above the assembly that each sampled 50,000 configurations with the first 10,000 steps discarded as equilibration. The resulting energy distributions as a function of angle are shown in Fig. S7 (obtained via standard inverse reweighting (19)). Note that rotation angles differing by 180° represent essentially equivalent orientations (an ideal double-helix structure was used for DNA, such that the symmetric phosphate backbone was directionless), but the entire range from 0° to 360° was sampled and treated fully, with no assumption of underlying symmetry. Nevertheless, the resulting distributions are highly symmetric with respect to offsets by 180° (see Fig. S7, *A* and *C*), which is a strong indicator of high convergence of simulations.

RESULTS

Design and modeling

The challenge in designing precise self-organization of molecular units on surfaces is to create cooperativity between contacts with the surface and interunit interactions, such that the assembly process is strictly surface-dependent. To choose an assembly topology suitable for such cooperativity, we followed the three selection rules established in our earlier study (20): 1) the assembly should consist of a common protein structural unit displaying a functional group physicochemically suitable for contacting the surface; 2) the unit should be patterned to mimic the geometry of the surface; and 3) the monomers should tile using energetically favorable intersubunit interactions that correspond to naturally designable protein-protein interfaces. Specifically, as our elementary unit, we chose a β-strand. To bias the sequence toward this conformation, we chose to alternate polar and apolar residues. Phe/Val residues in every second position were introduced to allow π-π/van der Waals interactions with graphene, respectively. Due to our interest in potential nucleic-acid binding properties of assemblies, we initially set the remaining (solvent-facing) positions of the peptide to Lys, but also considered other polar amino acids. We reasoned that these units could be patterned via nativelike β-sheet interactions to form a hydrophobic surface well suited for folding onto graphene. Such a mode of organization would be akin to amphipathic β-sheets folding onto hydrophobic cores in natural proteins or forming at artificial interfaces (21).

We next applied a series of structure-based computational modeling techniques to examine whether 1) the proposed sequence is indeed expected to prefer our hypothesized assembly (over other alternatives) and 2) such an assembly would be expected to form cooperatively, striking a balance between peptide-peptide and peptide-graphene interactions. To this end, we developed a method that avoided the direct enumeration of possible assembled conformations by adopting a hierarchical sampling approach. Inspired by the nucleation-growth model, the method envisions that a single peptide molecule may first spontaneously land on graphene and start sampling attached conformations, before beginning to assemble with other spontaneously adsorbed peptides (Fig. 1 *A*). The most favorable bound conformation for a single peptide is not necessarily also the best for assembly formation. However, it seems kinetically infeasible for an assembly to form out of extremely suboptimal/unlikely single-peptide conformations. We thus limited the search for potential assembly forming configurations to somewhat favorable graphene-bound single-peptide poses.

The overall modeling process consisted of two phases in which we first defined monomeric conformations at the graphene-water interface and then determined which of these could optimally assemble on the surface of graphene. In the first phase, we exhaustively sampled peptide backbone configurations and relative orientations with respect to graphene (Fig. 1 *A*), yielding a large list of favorable peptide/graphene poses. In the second phase, these poses were visited in ascending order of conformational energy, considering each as a potential assembly unit and sampling over

2D lattice parameters in P1 and P2 plane groups (with one and two peptides per unit cell, respectively); see Fig. 1 *B*. The top ~10^5 most energetically favorable poses from stage one were considered in stage two, covering a 40-kcal/mol range of single-peptide/graphene conformational energies. This balanced the thoroughness of the search with its computational complexity, given that stage-two calculations optimized over a large number of degrees of freedom (six assembly parameters for P2, in addition to side-chain conformations; see Materials and Methods).

As Fig. 1 *B* (*bottom*) shows, our design concept was borne out, yielding a parallel (P1) β-sheet assembly as the preferred lowest-energy conformation. Long in-register β-sheets, which we call β-tapes, align next to one other to fully cover the surface (Fig. S1). Notably, the conformation preferred by a single peptide on graphene was quite different from that required for assembly. Namely, the best peptide pose from stage one was a side-on attachment (Figs. S2 and 1 *B*, *top*), with side chains of both Phe and Lys making extensive hydrophobic contacts with the surface. On the other hand, the assembled state involved peptides in end-on conformations, with Phe side chains contacting graphene and Lys pointing into the solvent (Figs. S2 and 1 *B*, *bottom*). To further confirm this prediction of our assembly modeling framework, we computed conformational free energies of side-on and end-on ensembles for a single peptide, showing a ~15 kcal/mol preference for the former (see Materials and Methods). Explicit-solvent MD simulations also favored the side-on conformation (see Fig. S3). This strongly argued that the designed assembly would form highly cooperatively, requiring the presence of peptides in sufficient concentration for the end-on state to be appreciably populated.

Symmetry amplification

Graphene is periodic on an Ångstrom length-scale, so to a large (e.g., micron-sized) assembly it may appear as a quasi-flat, featureless surface. On the other hand, if the assembly itself is also atomically periodic, the combined superlattice can amplify graphene's Ångstrom-sized features by many orders of magnitude. To probe the magnitude of this effect, we sampled the rotation of the lowest-energy 2D lattice around a C6 axis of graphene, optimizing elevation, placement in the plane, and side-chain conformations each time. The resulting energy landscape shown in Fig. 1 *C* exhibits a 60° period, with significant energy wells that correspond to the six most preferred orientations (~0.5 kcal/mol for a short β-tape fragment of five peptides as in Fig. 1 *E*). We reasoned that over a longer assembly, these preferences would add up to a significant energy gap, giving a strict orientational preference, at least in the ground state. To confirm this expectation for a realistic assembly at room temperature, we ran extensive MD simulations of assembly fragments on graphene. As shown in Fig. 1, *D* and *E*, an individual five-strand β-tape shows a clear preference for the optimal alignment from the ground-state prediction, quickly switching to it when initialized in an orthogonal orientation. MD simulations of larger assembly fragments, with multiple short β-tapes interacting laterally, further verify this directional preference as individual β-tapes quickly reorient along the optimal axis (Fig. 1 *F*). Interestingly, rather than the entire assembly fragment reorienting in a concerted manner, initial lateral interfaces quickly dissociate, with individual domains sampling a variety of dockings as they rotate. Reoriented domains fuse to form extended β-tapes, indicating that lateral interfaces are significantly weaker than strand-strand interactions. Thus, although extended β-tapes are predicted to form, their lateral association at room temperature may vary from that in the ground-state model.

After the initial success with $(KF)_4$, the assembly modeling protocol was repeated for peptide $(KV)_4$ with a very similar resultant assembly geometry (data not shown). Further, we reasoned that other polar side chains in place of Lys residues would provide similar solvent-orientation preferences, so for experimental characterization we considered peptides with either Lys or Glu in solvent-exposed positions.

Peptides form organized assemblies with predicted topologies

We used high-resolution AFM to characterize the morphology of our designed peptides on graphite. Fig. 2 *A* describes the assembly protocol, which consists of 10–20 min incubating of a droplet of peptide solution onto a graphene/graphite substrate, rinsing with water, and drying over a gentle stream of N_2 gas. The peptide sequences and their respective numeral designations are indicated in Fig. 2 *B*. A representative AFM image taken in air of peptide **2** incubated on a highly oriented pyrolytic graphite (HOPG) surface is shown in Fig. 2 *C*. The figure shows that the peptide coats most of the surface, although multiple voids are present throughout the layer. Interestingly, the shape of the voids is not circular but rather elongated and stripelike, with neighboring voids appearing to be oriented with respect to each other. Below the image we show its fast Fourier transform (FFT), which further indicates the amorphous nature of the overlayer structure, as well as a line profile through a large void in the film, which reveals an ~2.5-nm layer thickness. We confirmed selective peptide adsorption on graphene using AFM, attenuated total reflection Fourier transform infrared spectroscopy, and Raman microscopy (see Fig. S4).

Interestingly, upon rehydration in water we observe the slow formation of order within the adsorbed layer highly consistent with the designed model. In Fig. 2 *D* we show an AFM image of the layer taken in water after an ~20-min rehydration period. The morphology of the hydrated film is

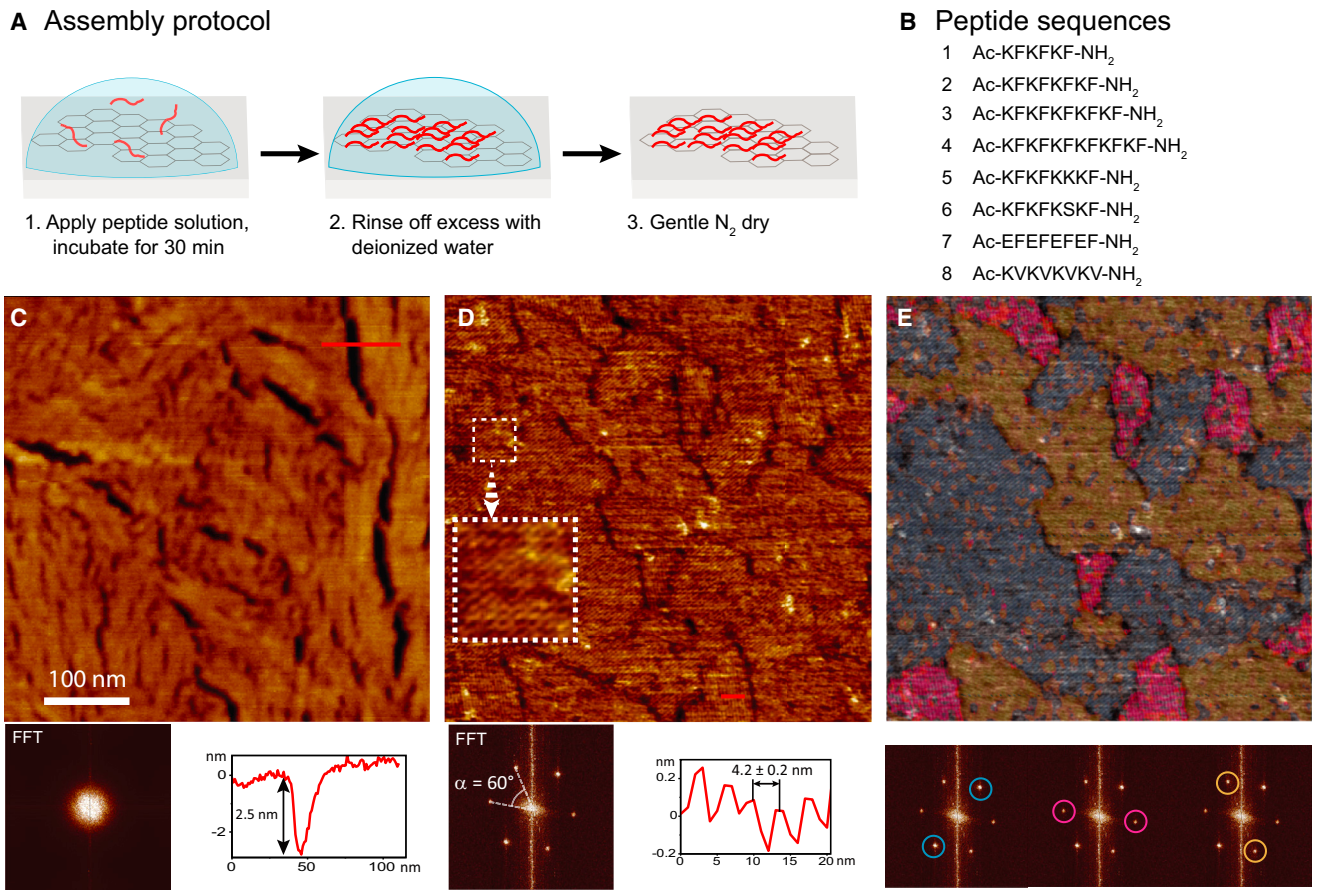

FIGURE 2 Designed peptide assemblies with long-range order. (*A*) Assembly protocol to obtain dry peptide assemblies on graphene/graphite. (*B*) Sequences of the peptides tested in this article. (*C*) AFM image of peptide **2** in air. FFT image and line cross section through an area that contains a void are also shown below the image. (*D*) AFM image of the same sample while the sample has been immersed in water for ~20 min (same scale as in *C*), as well as FFT and line cross section. A 2× magnified view of an area (*dashed square*) reveals a periodic structure that consists of rows with a spacing of 4.0–4.5 nm, and the FFT reveals ordering in six directions with C_6 symmetry. (*E*) Selected peak-pair inverse-FFT mapping of the peptide domains. Each color represents the inverse-FFT of each set of diametrically opposite peaks (see *colored circles* below the image). To see this figure in color, go online.

vastly different from the dry sample: large voids have disappeared, and there is evidence of boundary lines throughout. A closer view of the sample (*dashed white box*) reveals that the boundaries are the edges of distinct domains of crystalline nature: rows with a repeating pitch are observed within each domain, and the orientations of the rows are different in each domain. In contrast to the dry sample, the FFT shown underneath the image reveals six sets of equidistant, C_6-symmetric peaks. The reciprocal distance of the FFT peaks corresponds to a 4.0–4.5 nm spacing, in agreement with a line profile drawn through a section of the image in Fig. 2 *D*. This length scale and the observed topology closely agree with the predicted β-tape assembly. The predicted C6 symmetry is borne out, suggesting an atomically periodic assembly. The spacing between adjacent β-tapes predicted from the optimal ground-state assembly structure is 3.0 nm (see Fig. 1 *F*, *top left*)—significantly lower than the periodicity of ~4.2 nm observed in AFM line cross sections (Fig. 2 *D*, *bottom*). The additional 0.5–0.6 nm spacing on either side of each β-tape may be explained by moderate hydration pressure between the highly charged adjacent tapes, as observed with DNA fibers (22), which is not offset by any significantly attractive force. In fact, our room-temperature simulations showed inter-β-tape interfaces to be relatively weak, so that on average some gap between adjacent β-tapes is to be expected. Such gaps are also consistent with the observed height profiles from AFM line cross sections (Fig. 3, *A* and *B*).

In Fig. 2 *E*, we present a false color map of the domain orientation in the image, obtained by taking the inverse FFT of each set of peaks and coloring intense regions of the inverse FFT image using a different color. The map clearly shows that the boundaries represent domain borders in the layer, consistent with a nucleation-growth mechanism that is terminated when neighboring domains are encountered. Larger domains can be grown under nucleation-controlled conditions, e.g., at lower peptide concentrations, and repeated drying/rehydration of the peptide films could be performed multiple times to regenerate the organized structure with little to no degradation in coverage.

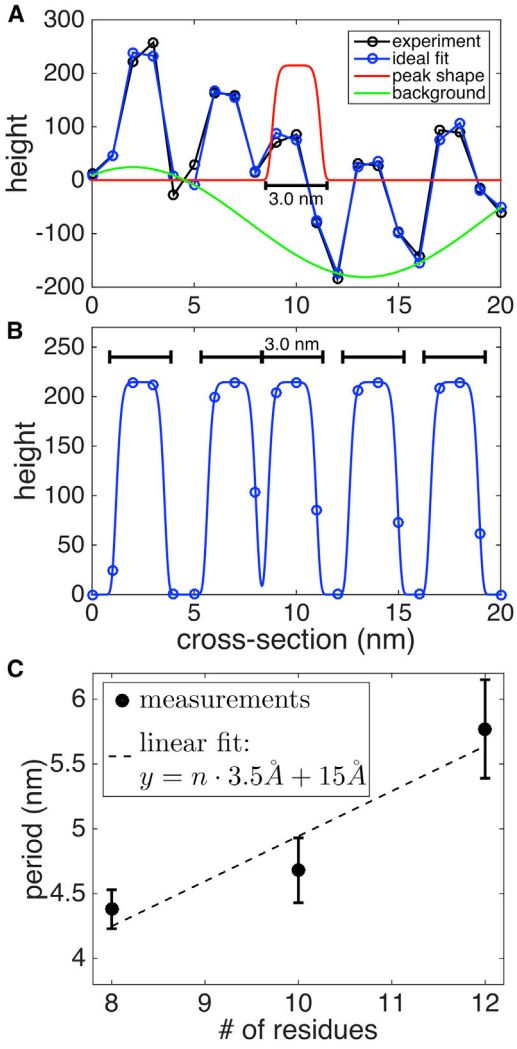

FIGURE 3 Agreement between predicted and observed β-tape periodicity. (*A*) A representative line cross-section profile observed in AFM (*black*) is fit to a sum of five peaks (modeled as generalized error distributions, *red*) on top of a varying height background (modeled as a sinusoid, *green*); final fit curve is shown (*blue*). The best-fitting peak shape (shape parameter of ~7.0) indicates a flat-topped distribution, such that gaps between adjacent peaks are expected. This is seen in (*B*), where the background is subtracted from the best-fit curve. (*Black bars*) Predicted β-tape width, 3.0 nm. (*C*) Error-weighted linear regression of AFM-derived row periodicity as a function of peptide length. To see this figure in color, go online.

Longer peptides further validate assembly topology

The computational model predicts that the rows observed in Fig. 2 *D* are β-tapes, with individual peptides oriented perpendicular to the direction of the rows. This suggests that row width is dictated by peptide length. We tested this hypothesis by characterizing assemblies of longer peptides consisting of 10 (**3**) and 12 (**4**) residues, in addition to the 8-residue peptide (**2**) already tested. If rows observed in AFM images indeed become broader, to the extent expected from the structural model, it would strongly support that the assembly topology is as predicted. Each of the longer peptides was subjected to the same assembly protocol and each gave very similar patterns in AFM. Cross-section height profiles were used to deduce the periodicity of assembly rows, as shown at the bottom of Fig. 2 *D* for **2**, with the results summarized in Fig. 3 *C*. As expected, the period does increase linearly with peptide length, validating that peptides are oriented perpendicularly to the rows. Further, the slope of this increase is 3.5 Å per residue, remarkably close to the 3.2 Å expected from the computational model (i.e., the translation along the β-strand per residue in the optimal assembly structure). This strongly supports the notion that the rows in AFM are indeed β-tapes. Finally, linear regression of period-versus-length predicts a nonzero intercept of 15 Å, further supporting the notion of gap space between adjacent β-tapes (as suggested by room-temperature MD). In fact, considering this gap, the row period of 4.4 $\pm$ 0.2 nm observed for **2** corresponds to a row width of ~2.9 nm, a nearly perfect match for the 3.0-nm β-tape width expected from the computational model.

Assembly is sequence-dependent with defined kinetics

To explore the impact of peptide sequence on the organization capability, we studied the assembly kinetics of positive and negative control peptides. To do so, we first incubated an HOPG substrate with peptide solution, rinsed/dried the sample, and immediately after rehydration we acquired multiple consecutive images of the sample. We quantified peptide organization by measuring the relative change in FFT peak intensity, ΔS_{FFT}, as a function of the scan time. In Fig. 4 *A* we plot the organization kinetics for five different 1 mM solutions of 8-mer peptide sequences: peptides **2** and **7** have alternating Lys/Phe and Glu/Phe residues, respectively, whereas in peptide **8**, Lys/Val alternate (i.e., no aromatic residues). In addition, in peptides **5** and **6**, the alternating sequence is broken by replacing the sixth Phe, a residue-facing graphene in the model, with a Lys (charged) and Ser (polar) residue, respectively. We find that upon rehydration all alternating peptides (**2**, **7**, **8**) begin to organize, and full organization occurs within 20 min (see AFM snapshots for assembly of **7** in Fig. S5). In contrast, while repeated imaging of peptides **5** and **6** revealed peptide adsorption, no organization was observed. These single mutants validate the graphene interface in the computational model, and show that self-organization of these biomolecules is strongly sequence-dependent.

Assembly topology is highly stable

Next, we tested the stability and morphology of the peptide layers under various experimental conditions. Plots of the row spacing (*d*) for a layer of peptide **2** as a function of pH and temperature are presented in Fig. 5, *A* and *B*,

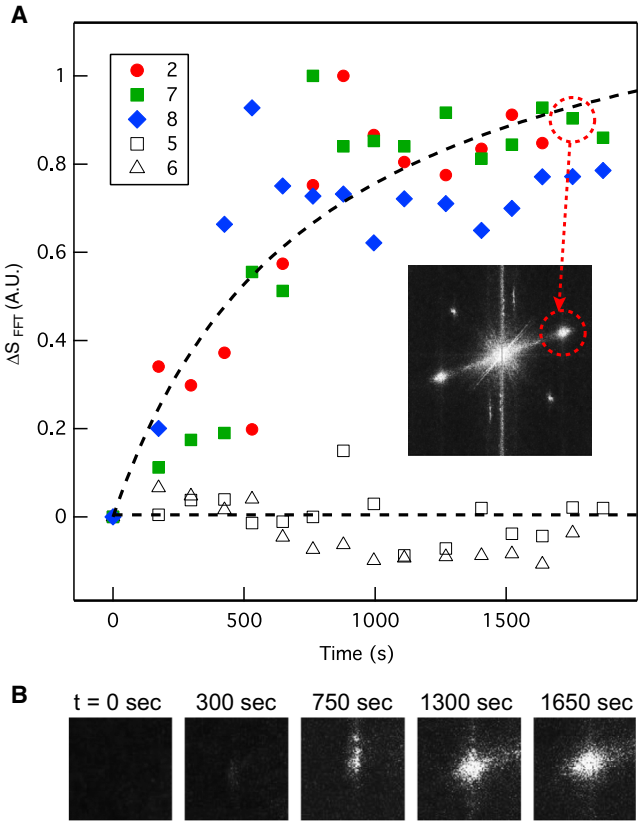

FIGURE 4 Assembly kinetics and sequence dependence. (*A*) Normalized change in FFT peak intensity as a function of time upon rehydration of adsorbed peptide films at $t = 0$ s. (*Inset*) FFT of one of the images in the plot (indicated by *red circle*). (*B*) Zoomed-in view of one of the FFT peaks at different times after rehydration of a layer of peptide **7**. To see this figure in color, go online.

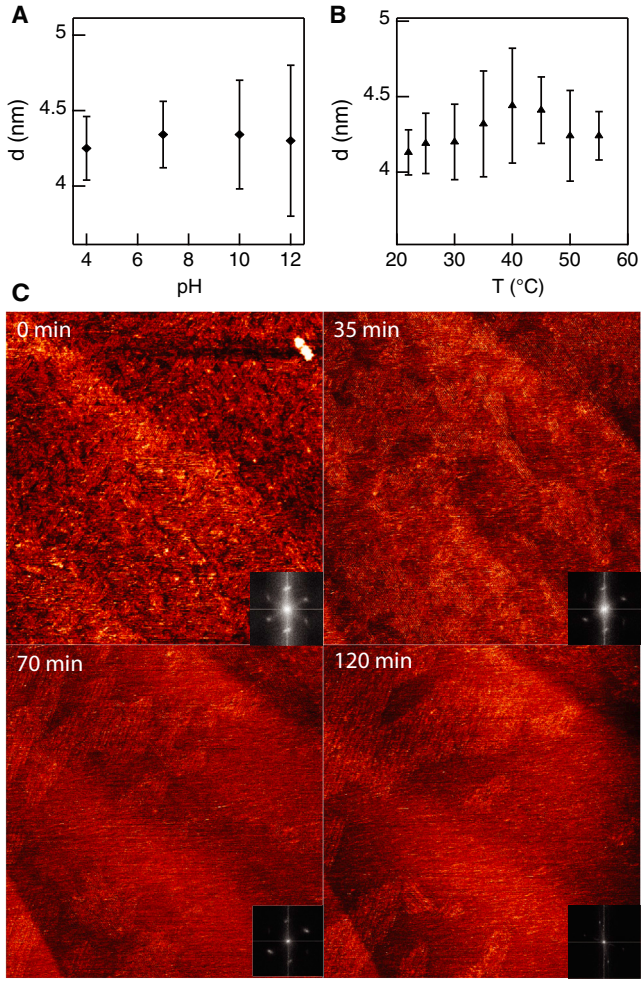

FIGURE 5 Stability to extreme buffer conditions. (*A*) Spacing (*d*) of peptide layer **2** (obtained from FFT of images) under >30-min incubation in solutions of different pH values. (*B*) Similar to (*a*), except that temperature was the changing parameter (obtained at pH 7). (*C*) Representative AFM images of peptide **2** taken from a time-series under incubation in 8 M urea at indicated times. (*Insets*) FFTs of the respective images. To see this figure in color, go online.

respectively. Each point in the plot was acquired from AFM images after >30 min incubation at each experimental condition. We find that the layers remain intact with high coverage, maintaining their coating uniformity and a constant spacing of 4.2 ± 0.3 nm throughout the pH range 4–12 and temperature range of 21–55°C. These results highlight the compatibility of the peptide layers with extreme environments. We did not test stability at higher temperatures due to experimental limitations in the AFM instrument that led to prohibitive thermal drift. Fig. 5 *C* shows four representative images taken during exposure of the peptide film to an 8 M solution of urea, a well-known protein denaturant. To obtain these data we first imaged the film under water, and then replaced the water via perfusion with 8 M urea before obtaining a consecutive series of 29 images. Remarkably, film degradation only became significant after ~45 min, as observed by the formation of large vacancies in the peptide film. Coupled to this urea-induced degradation is the formation of larger, more well-defined peptide domains in the remaining layer. We hypothesize that this is due to a destabilization of the assembled state, which leads to a more rapid desorption/regrowth equilibrium in the film, generating larger domains.

Stability of the peptide films to proteolytic degradation was also investigated. We incubated a surface coated with peptide **2** with a 2 μg/mL solution of proteinase K (a common nonspecific peptidase) and obtained consecutive images of the film to probe degradation, as shown in Fig. 6. Further, this experiment was performed for a high-coverage assembly of **2** (Fig. 6, *A–C*), as well as a low-coverage assembly that is characterized by many pinholes in the layer (Fig. 6, *D–F*). The results are striking: while more and more protease molecules adsorb to the high-coverage assembly, the coverage fraction does not degrade with time during the course of the experiment. In contrast, the pinhole-containing assembly degraded much faster, evidenced by formation of larger pinholes in the assembly. Additionally, we observed that protease prefers to bind to the peptides at pinhole boundaries. This suggests that the peptides are

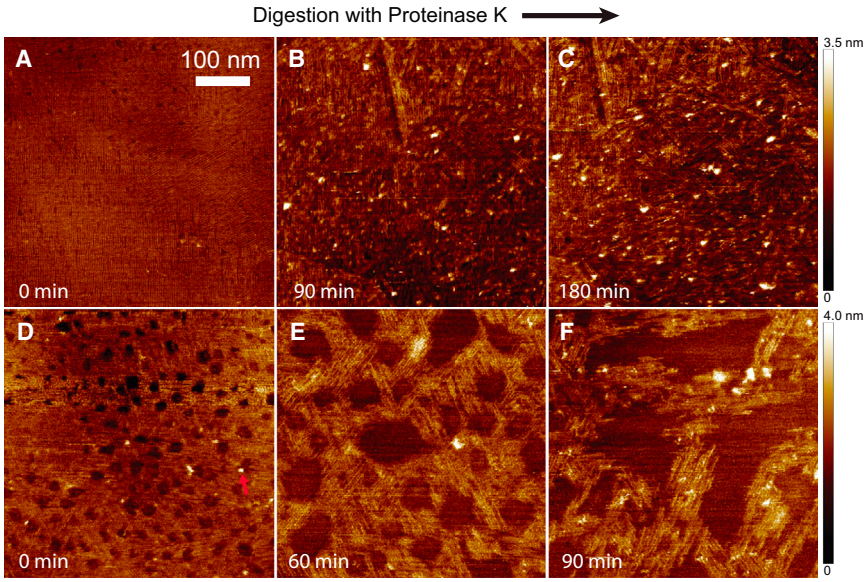

FIGURE 6 Stability to Proteinase K digestion. (*A–C*) Time-course AFM images of a high-coverage layer of assembled peptide **2** during a prolonged incubation with proteinase K solution. (*D–F*) Similar time-course experiment for a low-coverage layer of **2**. The high features (*white dots*) correspond to proteinase K molecules that are adsorbed onto the film (see *red arrow*). Scale bar in (*A*) is valid for all images. To see this figure in color, go online.

more susceptible to proteinase-mediated degradation when proteinase can access the side of the peptide, rather than its top face.

Assembly directs DNA binding

Our designed assemblies are effectively transforming the properties of the underlying graphene surface, while propagating its symmetry. Further, resultant surface properties were shown to be tunable via the identity of the surface-exposed amino acids. For example, with the peptides presented already in this study, the surface can be made either poly-cationic or poly-anionic. As a first step toward demonstrating the new capabilities this can provide, we sought to characterize the adsorption of DNA to our cationic peptide assemblies (peptides **2** and **8**). As a negatively charged molecule (due to its phosphate backbone), we reasoned that DNA should attach efficiently onto these assemblies. Calculations supported this expectation, as a 20-basepair DNA double helix initialized at >20 Å away from the surface, rapidly descended toward, and attached, to the peptide layer within 1 ns of MD simulation. In Fig. 7, we show AFM images of 900-bp double-stranded DNA on an assembly of **2** on HOPG (*A*), and 2000-bp DNA on an assembly of **8** on HOPG (*B*). Clearly, DNA does attach to these assemblies, although it did not attach to HOPG itself (data not shown). More strikingly, however, as is clear from the zoomed-in views in Fig. 7, *A* and *B* (*insets*), DNA apparently prefers to align with the underlying peptide assembly along the β-tapes of individual domains. Below each AFM image we show the distribution of DNA segment orientation angles (weighted by segment length), with respect to the horizontal laboratory axis. The histograms clearly show peaks that indicate preferred DNA orientations. Dashed lines behind the histograms indicate the orientation angles of the underlying β-tapes (bins at 0 and 180° in the histogram on the right represent equivalent orientations). Clearly, DNA predominantly prefers to align with the peptide domains, and the most likely DNA orientations (*black asterisks*) coincide with the three β-tape domain orientations on the surface in both cases. Red asterisks correspond to most probable DNA orientations that do not correspond to underlying peptide orientations. Importantly, the DNA/peptide-assembly interactions are not limited to the surface of graphite, as we also observe orientation of 2000-bp DNA on an assembly of **8** on a transferred graphene flake (see Fig. S6).

We reasoned that if the observed DNA alignment preference is encoded by the underlying assembly geometry, then this feature should also emerge from calculations. However, longer MD simulations revealed that the DNA-to-peptide layer attachment was too strong to enable efficient equilibration of different orientations within a reasonable timeframe. In fact, we did not observe any significant change in DNA angle (from the initially specified orientation), even upon several hundred nanoseconds of MD. Thus, in an effort to characterize the general expected characteristics of DNA orientational preferences, we implemented a multicanonical Monte Carlo approach to sample the docking of rigid DNA onto the peptide layer (see Materials and Methods). This showed that rather strong orientational preferences were indeed expected, driven largely by electrostatics, and that these depended on minor details of the assembly geometry (see Fig. S7). In particular, using the optimal ground-state assembly geometry discovered in the design phase (Fig. 1 *B*) we found two strongly selected orientations. One of these was along the β-tape axis, as observed in AFM images, and the other at a 60° angle to it (Fig. S7 *A*). Although the two directions had by far the lowest energies, the latter was slightly preferred, owing to

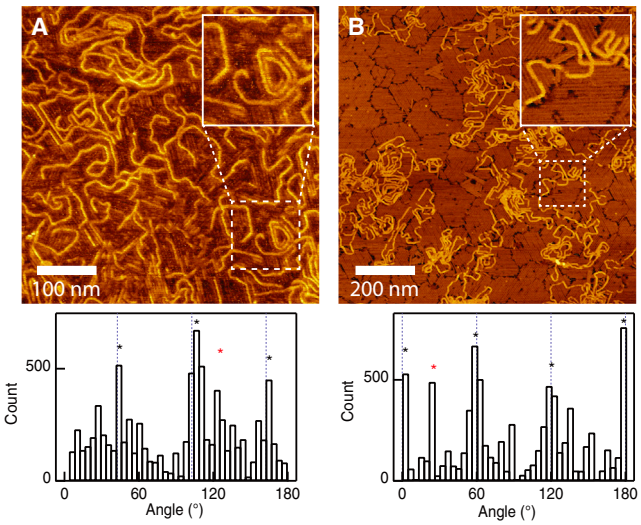

FIGURE 7 Peptide-directed DNA assembly. AFM images taken in fluid of (*A*) 900-bp DNA adsorbed on a layer of peptide **2** on HOPG, and (*B*) 2000-bp DNA adsorbed on peptide **8** on HOPG. Histograms below each image represent the weighted (by segment length) angular distribution of DNA contour length with respect to the horizontal axis, and vertical dashed lines highlight the measured peptide orientations. Asterisks denote the most probable aligned DNA segments (*black*) and the most significant misaligned DNA orientation (*red*). To see this figure in color, go online.

the fact that it enabled adjacent turns of the phosphate backbone to intercalate exactly between the amino groups of rows of Lys residues (Fig. S7 *B*). On the other hand, we had already suspected that in our ground-state model the packing of adjacent β-tapes was closer than that observed experimentally (Fig. 3). We thus also performed this calculation for an assembly geometry where the inter-β-tape spacing parameter was increased by 0.5 nm compared to the predicted ground state. Interestingly, in this case we again saw two strongly preferred alignments, but the orientation along the β-tape axis was now the dominant one (Fig. S7 *C*).

DISCUSSION

In this study we proposed and validated a design strategy for the cooperative assembly of peptides on graphitic surfaces, showing that calculations accurately anticipate the structure and major properties of the assembly. We further demonstrate that the tunability of the surface-exposed residues in the resultant assembly enables one to remodel surface properties, using this to create DNA-binding surfaces. Although amphipathic peptides have been shown to bind graphite, and long-range order has been observed in Yang et al. (23) and Brown et al. (24), this study is the first, to our knowledge, to provide an atomistic-level description of the resultant 2D crystalline state that is fully consistent with observations. We have also demonstrated that computation can be used to rationalize (and, ultimately, predict) emergent surface properties, such as an orientational preference for DNA interaction. This established the feasibility of using computation to anticipate and design precise crystalline assemblies of proteins on 2D nanomaterials. Finally, our study demonstrates the impressive capability of peptides to amplify symmetry: the Ångstrom-level periodicity of graphene is reflected at the micrometer scale in the clear directional preferences for the assembly of β-tape domains, which in turn encodes the observed long-range directional order of DNA binding to the surface of peptide assemblies.

As predicted, designed peptides form 2D monolayer crystals on the surface of graphene and graphitic interfaces, with anticipated topology. Formation of the crystals is designed to be a balance between interprotein and protein-surface interactions. Individual peptides prefer to adsorb to graphene in a conformation significantly different from that required for assembly. Peptides also do not spontaneously assemble in solution. Thus, formation of the 2D crystals proceeds strictly in a surface-dependent manner and only with sufficiently high concentration of peptide. When dehydrated, the peptide film shrivels due to competing air/hydrophobic and graphite/hydrophobic interactions in the absence of water. However, upon rehydration, the periodic arrays reform and the symmetry is preserved. The films are remarkably stable in a range of pH, urea concentration, and temperatures. Further, complete (pinhole-free) films of the peptide withstand enzymatic degradation by proteinase K. Surprisingly, aromatic groups in the hydrophobic side chain of the alternating peptide are not a prerequisite for peptide assembly.

An attractive aspect of coating surfaces with designed peptide layers is that it makes surface properties entirely tunable. As a simple demonstration of what this can enable, we showed that our cationic assemblies (but not the underlying HOPG) bound DNA. Furthermore, this binding occurred in an orientationally selective manner, whereby the DNA double helix preferred to align along assembled β-tapes. Extensive calculation revealed that this preference emerged from the underlying assembly symmetry and was largely driven by electrostatic DNA-peptide interactions. That this effect could be rationalized by molecular mechanics calculations opens up exciting prospects toward the design of surfaces in a manner that produces desired directional preferences in binding a host of polymeric and nonpolymeric materials.

CONCLUSIONS

The remarkable properties of our peptide-based assemblies and the success of our design and modeling approach motivate the broader application of computation toward the design of a large number of desired bio-nano assemblies. When combined with the appropriate surface (e.g., graphene nanodisk colloids), we envision a number of applications of these systems, including heterogeneous green catalysts, agents for bioimaging, and drug delivery agents for nanomedicine.

SUPPORTING MATERIAL

Supporting Materials and Methods and seven figures are available at http://www.biophysj.org/biophysj/supplemental/S0006-3495(16)30240-5.

AUTHOR CONTRIBUTIONS

G.-M.M. and Y.H.K. performed wet experiments; G.G. and J.Z. performed computational modeling; G.-M.M., J.Z., G.G., and M.W. analyzed the data; and G.-M.M., W.F.D., G.G., and M.W. wrote the article.

ACKNOWLEDGMENTS

We thank Marija Drndic for fruitful discussions.

This work was supported by National Science Foundation (NSF) grant No. EFMA-1542707 (to M.W.), National Institutes of Health grant No. GM54616 (to W.F.D.), NSF grant No. CHE-1413295 (to W.F.D.), NSF grant to the Laboratory for Research on the Structure of Matter, University of Pennsylvania (under DMR grant No. 1120901), an Alfred P. Sloan Fellowship to G.G. (under grant No. BR2013-038), NSF infrastructure grant CNS-1205521 to Dartmouth College, and National Research Foundation of Korea grant IBS-R015-D1.

REFERENCES

1. Cui, Y., S. N. Kim, …, M. C. McAlpine. 2010. Chemical functionalization of graphene enabled by phage displayed peptides. *Nano Lett.* 10:4559–4565.
2. Kim, S. N., Z. Kuang, …, R. R. Naik. 2011. Preferential binding of peptides to graphene edges and planes. *J. Am. Chem. Soc.* 133:14480–14483.
3. Katoch, J., S. N. Kim, …, M. Ishigami. 2012. Structure of a peptide adsorbed on graphene and graphite. *Nano Lett.* 12:2342–2346.
4. Khatayevich, D., C. R. So, …, M. Sarikaya. 2012. Controlling the surface chemistry of graphite by engineered self-assembled peptides. *Langmuir.* 28:8589–8593.
5. So, C. R., Y. Hayamizu, …, M. Sarikaya. 2012. Controlling self-assembly of engineered peptides on graphite by rational mutation. *ACS Nano.* 6:1648–1656.
6. Akdim, B., R. Pachter, …, B. L. Farmer. 2013. Electronic properties of a graphene device with peptide adsorption: insight from simulation. *ACS Appl. Mater. Interfaces.* 5:7470–7477.
7. Claridge, S. A., J. C. Thomas, …, P. S. Weiss. 2013. Differentiating amino acid residues and side chain orientations in peptides using scanning tunneling microscopy. *J. Am. Chem. Soc.* 135:18528–18535.
8. Zhang, Y., C. Wu, …, J. Zhang. 2013. Interactions of graphene and graphene oxide with proteins and peptides. *Nanotechnol. Rev.* 2:27–45.
9. Zhao, X., F. Pan, …, J. R. Lu. 2010. Molecular self-assembly and applications of designer peptide amphiphiles. *Chem. Soc. Rev.* 39:3480–3498.
10. Whaley, S. R., D. S. English, …, A. M. Belcher. 2000. Selection of peptides with semiconductor binding specificity for directed nanocrystal assembly. *Nature.* 405:665–668.
11. Zhang, S. 2003. Fabrication of novel biomaterials through molecular self-assembly. *Nat. Biotechnol.* 21:1171–1178.
12. Kulp, D. W., S. Subramaniam, …, A. Senes. 2012. Structural informatics, modeling, and design with an open-source Molecular Software Library (MSL). *J. Comput. Chem.* 33:1645–1661.
13. Lazaridis, T., and M. Karplus. 1999. Effective energy function for proteins in solution. *Proteins.* 35:133–152.
14. Lazaridis, T. 2003. Effective energy function for proteins in lipid membranes. *Proteins.* 52:176–192.
15. Brooks, B. R., C. L. Brooks, 3rd, …, M. Karplus. 2009. CHARMM: the biomolecular simulation program. *J. Comput. Chem.* 30:1545–1614.
16. Grigoryan, G. 2013. Absolute free energies of biomolecules from unperturbed ensembles. *J. Comput. Chem.* 34:2726–2741.
17. Phillips, J. C., R. Braun, …, K. Schulten. 2005. Scalable molecular dynamics with NAMD. *J. Comput. Chem.* 26:1781–1802.
18. Im, W., M. S. Lee, and C. L. Brooks, 3rd. 2003. Generalized Born model with a simple smoothing function. *J. Comput. Chem.* 24:1691–1702.
19. Janke, W. 1998. Multicanonical Monte Carlo simulations. *Phys. A.* 254:164–178.
20. Grigoryan, G., Y. H. Kim, …, W. F. DeGrado. 2011. Computational design of virus-like protein assemblies on carbon nanotube surfaces. *Science.* 332:1071–1076.
21. Rapaport, H., K. Kjaer, …, D. A. Tirrell. 2000. Two-dimensional order in β-sheet peptide monolayers. *J. Am. Chem. Soc.* 122:12523–12529.
22. Rau, D. C., and V. A. Parsegian. 1992. Direct measurement of the intermolecular forces between counterion-condensed DNA double helices. Evidence for long-range attractive hydration forces. *Biophys. J.* 61:246–259.
23. Yang, H., S.-Y. Fung, …, P. Chen. 2007. Modification of hydrophilic and hydrophobic surfaces using an ionic-complementary peptide. *PLoS One.* 2:e1325.
24. Brown, C. L., I. A. Aksay, …, M. H. Hecht. 2002. Template-directed assembly of a de novo designed protein. *J. Am. Chem. Soc.* 124:6846–6848.